J. Membrane Biol. 214, 165–180 (2007)
DOI: 10.1007/s00232-006-0068-4

The Journal of
Membrane
Biology

© Springer Science+Business Media, LLC 2007

Multiple Conductance Substates in Pharmacologically Untreated Na^+ Channels Generating Persistent Openings in Rat Entorhinal Cortex Neurons

Jacopo Magistretti[1], **Angel Alonso**[2]*
[1]Dipartimento di Scienze Fisiologiche-Farmacologiche Cellulari-Molecolari, Università degli Studi di Pavia, Via Forlanini 6, 27100 Pavia, Italy
[2]Department of Neurology and Neurosurgery, McGill University and Montreal Neurological Institute, 3801 University Street, Montréal, H3A 2B4, Québec Canada

Received: 24 August 2006/Revised: 20 December 2006

Abstract. Na^+-channel activity recorded in cell-attached patches from entorhinal cortex neurons in the absence of gating-modifying drugs was examined to determine the possible occurrence of substate openings. Brief sojourns to subconductance levels were occasionally observed within prolonged (''persistent'') burst openings. Subconductance occurrence and amplitude were determined following two distinct, complementary approaches: (1) direct visual inspection and (2) automated detection by application of a method that exploits the current variance of fixed-width tracing segments to sort amplitude estimations. The two approaches led to comparable results. At least six subconductance levels in addition to the full open state were revealed, with amplitudes that were approximately 20%, 30%, 40%, 50%, 60% and 75% that of full openings. The global probability of subconductance opening occurrence within a burst as well as the probability of observing one particular subconductance level within a burst showed no clear dependence upon membrane potential in the −40 to +10 mV range. Open- and closed-time distributions of substate openings could either be similar to those observed in burst full openings or show distinct patterns. Low-amplitude late openings were also observed in isolation, separately from full-size openings. These openings corresponded to conductance levels very similar to those of the substates observed within full-size burst openings; therefore, they were interpreted as isolated subconductance openings. Early, transient openings responsible for the fast-inactivating whole-cell Na^+-current component also manifested distinct conductance levels, the two most prominent of which were in an approximate 75:100 amplitude ratio. Interestingly, the 75% conductance level observed among early openings occurred much more frequently than in ''persistent'' burst openings. We conclude that pharmacologically untreated Na^+ channels from native neurons generate substate openings that may influence differently the multiple gating modes displayed by these channels.

Key words: Sodium channel — Substate — Persistent opening — Entorhinal cortex — Patch clamp — Cell-attached

Introduction

The gating activity of several ion channel types can show, in addition to a current amplitude level corresponding to the fully open channel, one or more lower-amplitude levels indicating the existence of conductance substates (Fox, 1987; Meves & Nagy, 1989). In some cases (e.g., various types of Cl^- channels), such subconductance levels report the presence of multiple permeation units arranged in parallel within a single channel. In other cases, conformational changes that modify the conductance properties of a single permeation path are believed to be implicated. Voltage-gated Na^+ channels have also been recognized to generate subconductance openings. In particular, Na^+ channels from heart myocytes (Nilius, Vereecke & Carmeliet, 1989; Schreibmayer, Tritthart & Schindler, 1989; Schreibmayer & Jeglitsch, 1992), skeletal muscle fibers (Patlak, 1988; Naranjo & Latorre, 1993) and neuroblastoma cells (Chinn & Narahashi, 1986; Nagy, 1987), as well as Na^+ channels isolated from mammalian forebrain and reconstituted into planar lipid bilayers

Correspondence to: J. Magistretti; email: jmlab1@unipv.it
*Angel Alonso is deceased.

(Green, Weiss & Andersen, 1987), have been investigated and found to generate subconductance openings in addition to a dominant full-conductance level. In the above studies, Na^+ channels were treated with gating-modifying drugs and toxins able to suppress channel inactivation, including batrachotoxin, sea anemone toxin II (ATx II), brevetoxin 3, deltamethrine, veratridine, chloramine T and DPI 201–106. By stabilizing the normally short-lived Na^+-channel openings, these agents make substate detection easier. However, whether or not such gating modifiers may have a causal role in inducing subconductance levels or in modifying the properties of substate openings is difficult to firmly establish. Although in some cases similar subconductance levels were observed in the presence of different gating modifiers (Nagy, 1987; Schreibmayer et al., 1989), some discrepancies have been observed in other cases. For instance, in skeletal muscle Na^+ channels, a subconductance level equal to ~35% of the fully open state conductance was most frequently observed in the presence of DPI 201–106 (Patlak, 1988), whereas a 75% subconductance level was found to be dominant in the presence of batrachotoxin (Naranjo & Latorre, 1993). In neuroblastoma cells, Na^+ channels treated with deltamethrine showed a subconductance level equal to ~66% of the full conductance (Chinn & Narahashi, 1986), whereas ATx II and chloramine T revealed 25%, 50% and 80% subconductance levels (Nagy, 1987). External agents can indeed have a causal role in the appearance of substate channel openings. For instance, in heterologously expressed Na^+ channels from chick neurons, veratridine was found to prominently induce long-lasting, low-amplitude openings of conductance equal to ~24% that of the normal open state (Sigel, 1987). In cardiac Na^+ channels, Zn^{2+} induces an ~15% subconductance level (Ravindran, Schild & Moczydlowski, 1991) that has been attributed to a channel conformational change to a low-conductance state (Schild, Ravindran & Moczydlowski, 1991). Although substate openings have also been occasionally reported in the absence of gating modifiers (Patlak, 1988), a systematic study of substate patterns in untreated Na^+ channels has never been carried out.

In previous studies by our group, sustained Na^+-channel activity responsible for the persistent component of voltage-dependent Na^+ current (I_{NaP}) has been characterized in rat entorhinal cortex layer II neurons. This activity mainly consisted of prolonged and/or late burst openings (Magistretti, Ragsdale & Alonso, 1999a), characterized by strong voltage dependence of mean intraburst open time (Magistretti & Alonso, 2002). We also found that the average conductance of "persistent" burst openings was higher than that of early openings responsible for the transient Na^+-current component (~20 *vs.* ~15 pS) (Magistretti et al., 1999a; Magistretti, Ragsdale & Alonso, 1999b). In the present study, we exploited the spontaneous occurrence of persistent burst activity to evaluate the presence of subconductance levels in Na^+ channels from native entorhinal cortex neurons independently of gating-modifying agents. In particular, we investigated (1) the occurrence of subconductance openings both within full-amplitude burst openings and in isolation, (2) the kinetic properties and possible voltage dependence of subconductance openings and (3) the possible relation between subconductance levels and low-conductance openings underlying the transient Na^+-current component. We found that multiple subconductance levels, ranging from ~20% to ~75% of the full-conductance level, are present in the Na^+ channels under study and appear both within full-size burst openings and as isolated late openings. We also provide data compatible with early, transient low-conductance openings corresponding to one such subconductance level.

Materials and Methods

Cell Preparation and Patch-Clamp Recordings

Acutely isolated neurons were prepared from layer II of entorhinal cortex from young adult Long-Evans rats (P25–P35). The details on the dissection procedure followed, and the enzymatic and mechanical dissociation method applied are described elsewhere (Magistretti & de Curtis, 1998; Magistretti et al., 1999a; Magistretti & Alonso, 2002). After isolation, cells were seeded on a recording chamber mounted on the stage of an inverted microscope (Axiovert 100; Zeiss, Oberkochen, Germany) and observed at ×400 magnification. Cells were initially perfused with a standard *N*-(2-hydroxyethyl)piperazine-*N*′-(2-ethanesulfonic acid) (HEPES) buffer containing (in mmol/l) 140 NaCl, 5 KCl, 10 HEPES (free acid), 2 $CaCl_2$, 2 $MgCl_2$ and 25 D-glucose (pH 7.4) with NaOH, bubbled with pure O_2. Single-channel patch pipettes were prepared from thick-wall glass capillaries, coated with Sylgard® (Dow Corning, Midland, MI) and filled with a solution containing (in mmol/l) 130 NaCl, 35 tetraethylammonium (TEA)-Cl, 10 HEPES-Na, 2 $CaCl_2$, 2 $MgCl_2$ and 5 4-aminopyridine (pH 7.4) with HCl. Patch pipettes had resistances ranging 10–35 MΩ when filled with the above solution. After obtaining the cell-attached configuration, the extracellular perfusion was switched to a high-potassium solution containing 140 K-acetate, 5 NaCl, 10 HEPES (free acid), 4 $MgCl_2$, 0.2 $CdCl_2$ and 25 D-glucose (pH 7.4), with KOH to hold the neuron resting membrane potential near 0 m*V*. Recordings were performed at room temperature using an Axopatch 200B amplifier (Axon Instruments, Foster City, CA). Capacitive transients and linear current leakage were minimized online by acting on the respective built-in compensation sections of the amplifier. To elicit voltage-gated Na^+-channel currents, depolarizing protocols consisting of 500-ms or 50-ms depolarizing voltage steps were applied. To avoid cumulative channel inactivation, voltage steps were delivered every 5.6 s. The holding potential was −100 m*V*.

Data Acquisition

Voltage protocols were commanded and current signals acquired with a Pentium PC interfaced to an Axon TL1 interface, using the Clampex program of the pClamp 6.0.2 software package (Axon Instruments). Current signals were filtered online using the amplifier's built-in low-pass filter (4-pole low-pass Bessel filter, with

signal attenuation, above the −3 dB frequency, of 24 dB/octave) at a cut-off frequency dependent on the acquisition frequency. Currents evoked with 500-ms depolarizing pulses were filtered at 2 kHz and digitized at 10 kHz; currents evoked with 50-ms pulses were filtered at 5 kHz and digitized at 100 kHz.

Data Analysis: Substate Detection

Single-channel recordings were analyzed using Clampfit (from the pClamp 6.0.5 software package, Axon Instruments). Residual capacitive transients were nullified by offline subtracting fits of average blank tracings. Residual leakage currents were carefully measured in tracing regions devoid of any channel openings and digitally subtracted.

The analysis of Na^+-channel conductance substates was carried out by adopting two complementary approaches:

1. The first approach consisted of visual inspection of tracings to detect substate openings occurring either within a burst full opening or in isolation. Once a presumed substate opening was identified, one or more tracing segments were selected over which the subconductance level was considered stable and unequivocal, based on the following criteria: (i) absence of visible transitions to the closed state or other open states or superimposition of openings due to other channels, (ii) amplitude fluctuations similar to the baseline background noise level and (iii) duration ≥1.0 ms. The substate opening amplitude was then measured by averaging the data points contained in such segment(s). Current variance (s^2) was also calculated for comparison with the s^2 values observed in correspondence with the baseline or full channel openings (see Results).
2. The second approach consisted of application of the variance-mean analysis method introduced by Patlak (1988). This method consists of creating, in each digitized current tracing, a "window" of fixed width equal to n consecutive sample points over which the mean, I_{avg}, and s^2 are calculated. The window is shifted point by point along the time axis, and for each shift a new I_{avg} and a new s^2 are calculated. A family of I_{avg}/s^2 pairs is thus obtained, and each pair is accepted or rejected based on comparison of s^2 with a preset upper limit value corresponding to the baseline s^2. This conservative criterion allows one to sort out a number of I_{avg} values corresponding to stable channel-gating states (full openings, substate openings or closings), while discarding values influenced by state transitions, flickering and/or superimposed openings. In our analysis, the sliding window consisted of 10 consecutive points (corresponding to 1 ms at an acquisition frequency of 10 kHz). An automated routine performing the above analysis was compiled in the Labview environment (National Instruments, Milan, Italy). The data thus obtained were used to construct I_{avg} frequency distribution diagrams.

Histograms were fitted with single gaussian functions or the sum of more gaussians in the following form:

$$y = \sum_{j=1}^{m} \frac{A_j}{\sigma_j\sqrt{2\pi}} \exp\left[-(x-\mu_j)^2/2\sigma_j^2\right], \quad (1)$$

where σ is the standard deviation and μ is the mean. Fittings were carried out using the fitting routine of Origin 6.0 (MicroCal Software, Northampton, MA), based on a minimum-χ^2 method. All average data are expressed as mean ± standard error of the mean (SEM), unless otherwise specified.

Dwell Time Analysis

Channel dwell times were determined by applying a standard half-amplitude crossing protocol using Fetchan (pClamp 6.0.5). Because in the present study's context the aim of the analysis was to compare gating kinetics during subconductance openings *vs.* full-size burst openings, dwell time event lists were obtained from each recording by separately analyzing subconductance openings and full-size openings in independent sessions. Background noise is expected to have a greater influence on dwell time determination when the difference between two imposed current levels is smaller. To avoid the biases introduced by this effect, we proceeded as follows. An event list was created for a specific subconductance opening after fixing the corresponding amplitude level, A_s. Then, two new amplitude levels were defined, one corresponding to that of the full-size openings, A_o, the other equal to $A_o - A_s$, and a new event list was generated for full-size burst openings from the same recording. In this way, the influence of background noise on state-transition detection was the same when subconductance openings and full-size openings were analyzed. No minimum-duration threshold for detection of state transitions was imposed. With the low-pass filtering cut-off frequency used (2 kHz) and assuming that the filter output approaches that of a gaussian filter, a theoretical "dead time" for event detection of 90 μs is predicted (Colquhoun & Sigworth, 1995).

To analyze channel open and closed times, logarithmic frequency-distribution graphs of the same quantities were then constructed (*see* Blatz & Magleby, 1986; Sigworth & Sine, 1987; McManus, Blatz & Magleby, 1987; Magistretti & Alonso, 2002; Magistretti, Ragsdale & Alonso, 2003). To do this, lower and upper bin limits were first set according to a logarithmic scale that yielded 11.4 bins/decade. To avoid arbitrary over- or underestimations of the calculated numbers of events per millisecond, the upper limit value of each bin was approximated to the nearest tenth of a millisecond above so as to make each bin width equal an integer multiple of the sampling interval routinely used (100 μs). After data binning, the natural logarithm of the number of observations per time unit was calculated for each bin. The values thus obtained were plotted as a function of $x = \ln t$ to construct log-log frequency-distribution graphs. Due to the dead-time value holding under our experimental and analytical conditions (90 μs, *see above*), which did not warrant consistent detection of transitions lasting ∼100 μs, events consisting of only one 100-μs sample were excluded from histograms and not considered for fitting. Exponential fitting of log-log histograms was carried out by applying the following double logarithmic transform of a sum of exponential functions (*see* Magistretti & Alonso, 2002):

$$y = \ln\left\{\sum_{j=1}^{m} \frac{W_j}{\tau_j} \exp\left[-\exp\left(x - x_{0j}\right)\right]\right\} \quad (2)$$

where $x_{0j} = \ln \tau_j$ and W_j and τ_j are the weight coefficient and time constant, respectively, of each exponential component. Fittings were performed using the fitting routine of Origin 6.0 based on a minimum-χ^2 method. Logarithmically binned histograms constructed as described above were displayed on a linear time scale to obtain log-linear graphs, in which single exponential components are visually recognized as straight lines. Theoretical mean open times for individual subconductance openings or full-size burst openings ($\bar{\tau}_o$s) were derived from the exponential fitting functions obtained from open-time histograms according to the following relationship:

$$\bar{\tau}_o = \sum W_i \cdot \tau_j / \sum W_j \quad (3)$$

The same method was adopted to calculate theoretical mean closed times ($\bar{\tau}_c$s).

Results

Long-lasting (500 ms) step depolarization at −50 to +10 mV applied from a holding potential of −100

mV activated Na^+-channel activity that consisted in clustered early openings, responsible for the classical transient Na^+ current (I_{NaT}), followed by late and/or prolonged burst openings, underlying the persistent Na^+ current, I_{NaP} (Magistretti et al., 1999a; Magistretti & Alonso, 2002). The latter, "persistent" channel activity was first examined to verify the possible existence of channel substates.

Multiple Conductance Sublevels during Prolonged Burst Openings

Prolonged and/or late burst openings are characterized by a conductance of approximately 19–20 pS (Magistretti et al., 1999a). However, inspection of full-size burst openings revealed occasional, brief sojourns to conductance levels lower than that of the full open state (Fig. 1). Typically, such intraburst subconductance openings were both accessed from, and followed by, dwellings in the full open state; but in some cases a subconductance opening could be accessed directly from the baseline (see Fig. 2A3) or terminate with channel closure (see Fig. 1, no. 10). Subconductance openings appeared to occur at multiple amplitude levels relative to full-size openings (Fig. 1). To evaluate the existence of predominant conductance sublevels and determine their amplitude, two complementary approaches were adopted: (1) direct visual inspection of experimental tracings to search for stable subconductance and full-conductance openings and measure their amplitude and (2) automated analysis based on the variance-mean method introduced by Patlak (1988). Both methods are described in detail in Materials and Methods.

By applying method 1, current-amplitude values for subconductance and full-size openings were obtained by calculating mean current amplitudes of selected regions of the experimental tracings. Current variance (s^2) was also calculated in each measurement for comparison with baseline s^2 values. On average, s^2 was very similar for full-size openings ($0.0102 \pm 9.4 \cdot 10^{-4}$ pA^2), subconductance openings ($0.0106 \pm 1.04 \cdot 10^{-3}$ pA^2) and the corresponding baseline regions ($0.0093 \pm 7.8 \cdot 10^{-4}$ pA^2; $n = 70$ in all cases) ($P = 0.6$, one-way analysis of variance), thus confirming the reliability of our measurements based on method 1. The results of method 1 are illustrated in Figure 2. Subconductance openings of similar amplitude relative to the full-size opening could be occasionally observed at different test potentials in individual patches (Fig. 2A). This suggests that in the voltage window explored (−50 to +10mV) the amplitude of subconductance openings varies linearly with membrane potential, similarly to that of full-size openings (Magistretti st al., 1999a, 1999b). For this reason, measurements of subconductance opening amplitude, relative to that of full-size opening amplitude, were pooled even if obtained at different test potentials. The frequency distribution diagram of subconductance relative amplitude clearly revealed five distinct peaks (Fig. 2B), corresponding to

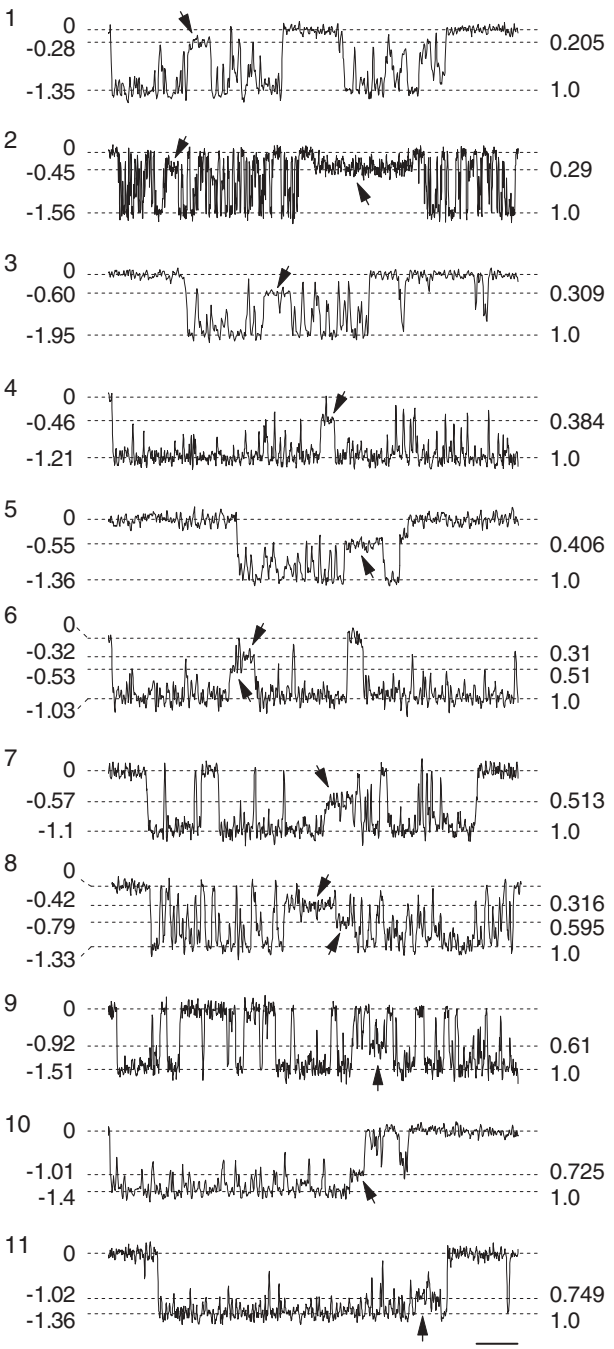

Fig. 1. Intraburst subconductance openings show multiple conductance levels. The figure shows representative examples of subconductance openings (*arrows*) occurring within 11 different full-size persistent burst openings. Recordings were made in nine different patches at various test potentials (V_{test}s) (−50 to −10 mV). The numbers to the left of each tracing are absolute current levels (pA). The numbers to the right of each tracing represent relative amplitude values (with the amplitude of full-size openings made equal to 1.0). x-axis calibration bar = 10 ms for tracings 1, 3, 5–7, 9 and 10; 12 ms for tracing 8; and 15 ms for tracings 2, 4 and 11.

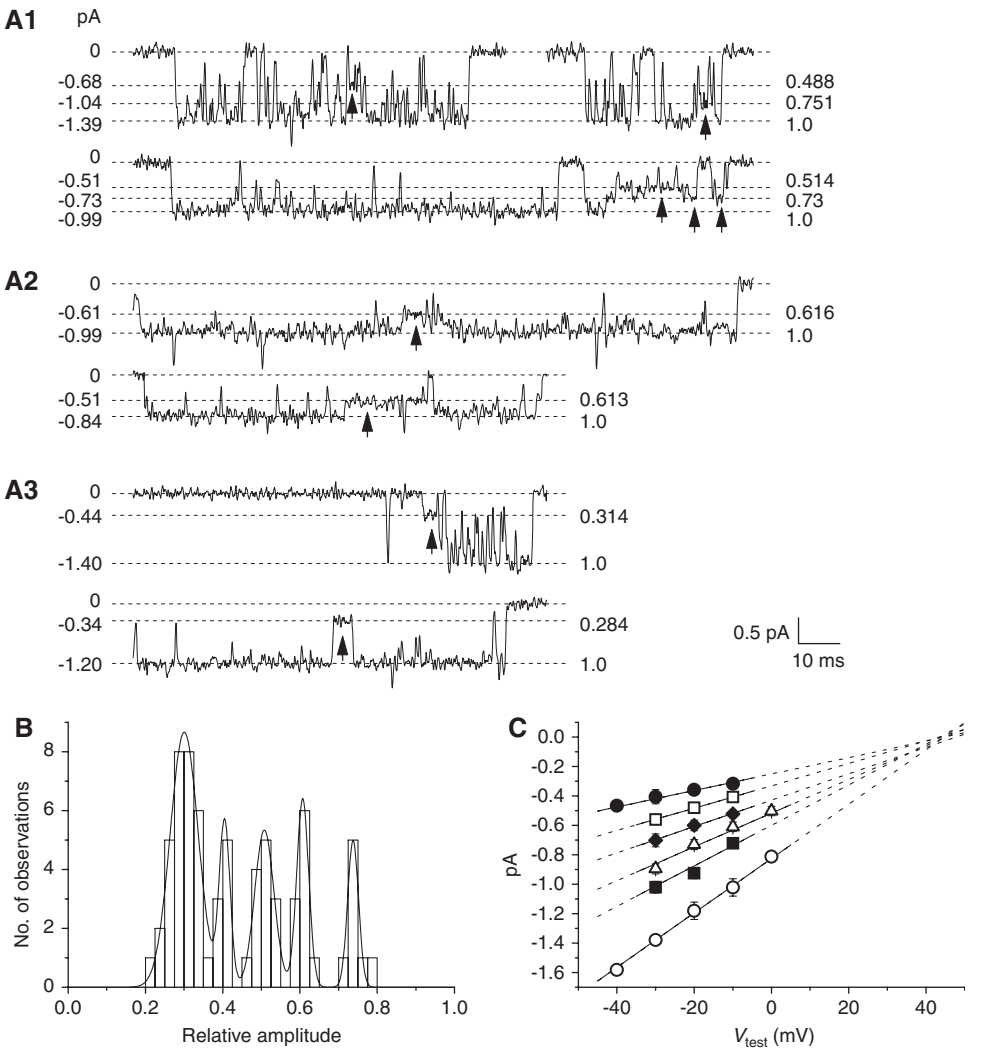

Fig. 2. Identification of multiple, discrete conductance levels among intraburst subconductance openings. (*A*) Examples of visually identified intraburst subconductance openings (*arrows*) recorded at various V_{test}s in three different patches (B9n01 in *A1*, A9n09 in *A2*, D9n09 in *A3*). V_{test}s were −30 m*V* in *A1* (*top*) and −10 m*V* in *A1* (*bottom*), −10 m*V* in *A2* (*top*) and 0 m*V* in *A2* (*bottom*), −30 m*V* in *A3* (*top*) and −20 m*V* in *A3* (*bottom*). The numbers to the left of each tracing are absolute current levels (pA). The numbers to the right of each tracing represent relative amplitude values (with the amplitude of full-size openings made equal to 1.0). Note that subconductance openings of similar amplitudes relative to full-size openings were observed in a single patch regardless of the different V_{test}s. (*B*) Frequency-distribution diagram of relative amplitudes of visually identified subconductance openings. Amplitude values are expressed as normalized to those of full-size openings. The data were obtained from 18 different patches, and measurements made at different V_{test}s were pooled. The histogram was best fit with the sum of five gaussian functions (see Eq. 1). Mean (μ) values returned by fitting were 0.3, 0.405, 0.508, 0.607 and 0.738. (*C*) Average *I-V* plots of subconductance levels and the fully open state. Subconductance openings that fell within one of the peaks of the histogram in *B* (specifically, with an amplitude comprised within the interval μ ± 0.05) were selected, average values were obtained in each patch, then averaged among patches and plotted as a function of V_{test}. Each point is the average of measures made in two to five patches, error bars are standard deviations (SD; where the error bar is not visible, SD is smaller than the size of the symbol). Slope conductance and extrapolated reversal-potential values were obtained by linear regression of data points (*straight lines*) and were 18.5 pS and +44.5 m*V*, respectively, for the fully-open state (*open circles*), 13.8 pS and +43.6 m*V* (*filled squares*), 11.5 pS and +45.1 m*V* (*open triangles*), 9.0 pS and +47.8 m*V* (*filled diamonds*), 7.6 pS and +43.5 m*V* (*open squares*) and 5.6 pS and +45.0 m*V* (*filled circles*).

approximately 30%, 40%, 50%, 60% and 75% of the full-size opening amplitude. Once such subconductance levels were identified, an average current-voltage (*I-V*) plot was constructed for each of them and compared with the *I-V* relationship of the fully open state (Fig. 2C). Linear regressions to data points returned similar values of extrapolated reversal potential for all subconductance levels and the fully open state. Relative amplitude values of subconductance levels, measured using slope coefficients returned by linear regressions, were 0.303, 0.412, 0.486, 0.621 and 0.746, (see Fig. 2C, legend). in good agreement with the estimations obtained from the analysis of pooled relative-amplitude data.

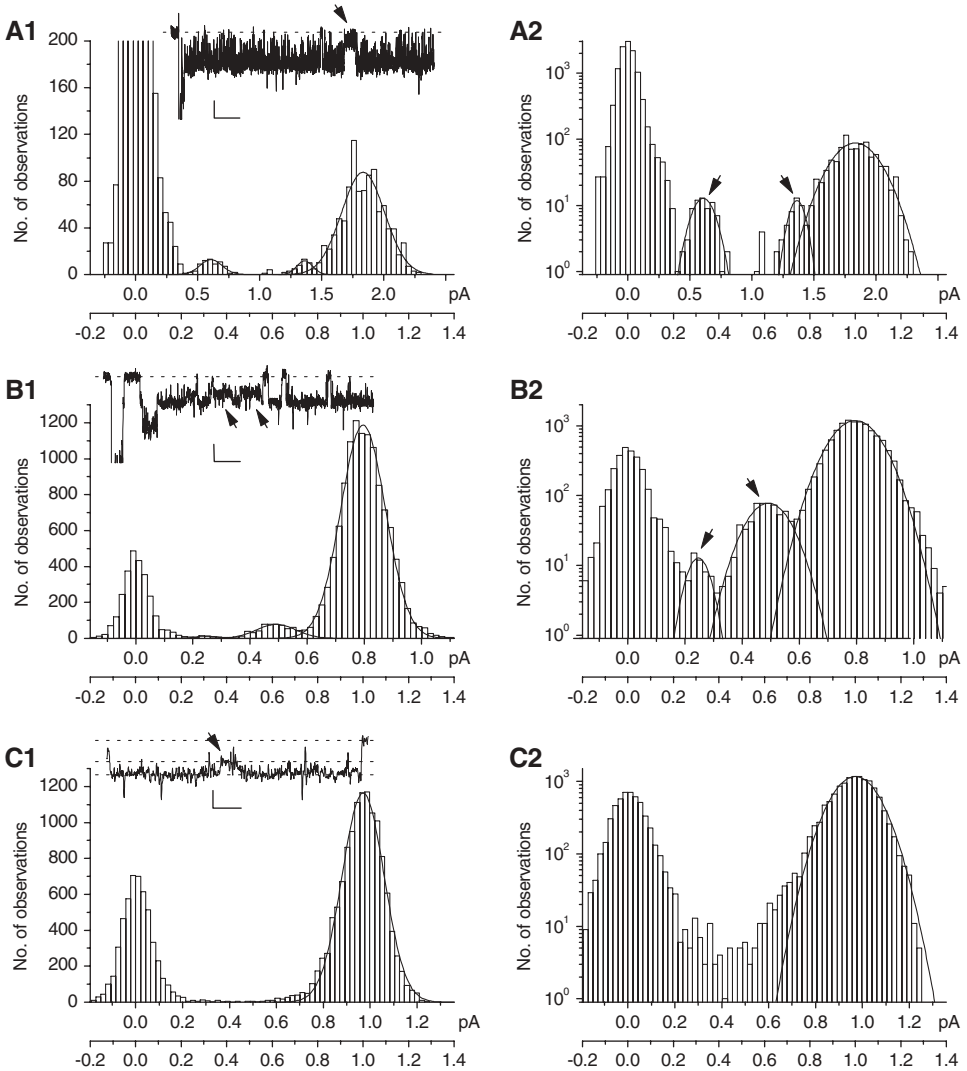

Fig. 3. Automated analysis of Na^+-channel burst openings reveals subconductance levels. The figure illustrates the histograms of amplitude estimates obtained by applying the Patlak variance-mean analysis (*see text for details*) to persistent Na^+-channel burst openings recorded in two representative patches. Experimental tracings were obtained at V_{test} of −40 m*V* in *A* (patch A8618), 0 m*V* in *B* (patch A9n09) and −10 m*V* in *C* (patch A9n09). Exemplary experimental tracings from each recording are shown in the insets of panels *A1*, *B1* and *C1* (calibration bars = 1.0 pA, 50 ms in *A1*; 0.5 pA, 50 ms in *B1*; 0.5 pA, 16 ms in *C1*); *arrows* point to visually identifiable subconductance openings. In each pair of histograms, numbers of observations are given in both linear scale (*left*) and logarithmic scale (*right*). The peaks corresponding to substate openings (*arrows*) and full-size openings were separately fitted with single gaussian functions (*smooth lines*). Fitting parameters are (*A*) A_1 = 2.85, μ_1 = 0.607 pA, σ_1 = 0.089 pA; A_2 = 1.89, μ_2 = 1.362 pA, σ_2 = 0.064 pA; A_3 = 30.08, μ_3 = 1.833 pA, σ_3 = 0.173 pA; (*B*) A_1 = 1.18, μ_1 = 0.235 pA, σ_1 = 0.037 pA; A_2 = 13.38, μ_2 = 0.48 pA, σ_2 = 0.069 pA; A_3 = 233.34, μ_3 = 0.784 pA, σ_3 = 0.078; (*C*) A = 245.86, μ = 0.914 pA, σ = 0.084 pA. The estimated amplitudes of full-size openings obtained from gaussian fittings were used to normalize all current amplitude values: in each histogram, the upper *x* axis gives absolute current values, whereas normalized current values are specified in the lower *x* axis. Note that subconductance peaks were clearly visible in some cases (*A* and *B*) but not in others (*C*).

To perform the Patlak variance-mean analysis (method 2), full-size burst openings of at least 25 ms in duration were selected. Isolated subconductance openings (*see below*) were excluded. The analysis returned histograms of amplitude estimates, and each histogram was constructed using data from bursts recorded in a single patch at the same test potential. In most cases (44 of 76) no clear, additional peaks besides that corresponding to the fully open state were observed. In the remaining cases, one or more additional peaks were present, thus revealing intraburst subconductance levels. Two such examples are illustrated in Figure 3A and B. The amplitude, both absolute and relative to that of the full open state, of subconductance levels was estimated by gaussian fitting of histogram peaks (*see* Fig. 3). Average values of relative amplitude levels are given in Table 1. It can be seen that the values returned by this analytical

Table 1. Average relative amplitudes of six distinct subconductance levels

	Intraburst substate openings		Isolated substate openings	
Level	Relative amplitude	*n*	Relative amplitude	*n*
1	0.202 ± 0.005	8	0.199 ± 0.004	6
2	0.306 ± 0.01	8	0.304 ± 0.002	12
3	0.41 ± 0.01	6	0.397 ± 0.002	10
4	0.508 ± 0.012	6	0.503 ± 0.002	11
5	0.599 ± 0.016	4	0.603 ± 0.003	8
6	0.76 ± 0.006	12	0.747 ± 0.006	7

Subconductance openings occurring within full-size burst openings (columns 2 and 3) and subconductance openings occurring in isolation (columns 4 and 5) are illustrated separately. Average values were calculated from the relative amplitude values returned by the analysis of amplitude estimate histograms such as those shown in Figures 3A, B and 9B.

procedure were very similar to those obtained from visual inspection, with an additional subconductance level at approximately 20% of full-opening amplitude. For comparison, Figure 4 shows histograms of pooled relative-amplitude data from the same recordings illustrated in Table 1.

It is worth noting that the information obtained from the two analytical approaches independently used to detect subconductance levels was complementary due to the sensitivity limitations of both methods. In particular, not in all cases in which the variance-mean analysis returned a subconductance peak in amplitude histograms could stable subconductance openings be unequivocally revealed by visual inspection. Conversely, not in all cases in which visual inspection clearly indicated the occurrence of a subconductance opening was a distinct peak present in histograms constructed from variance-mean analysis. An example of the latter case is illustrated in Figure 3C (*see also* Patlak, 1988).

The question then arose of whether the occurrence of subconductance openings was influenced by membrane potential. This issue was addressed by considering all amplitude histograms obtained with variance-mean analysis, whether they showed clear subconductance peaks or not. In each histogram, normalized by the full-opening amplitude, the numbers of observations in a defined relative-amplitude window were summed. Four windows were considered in the scale of relative amplitudes (A): (1) $0.25 \leq A < 0.35$, (2) $0.35 \leq A < 0.45$, (3) $0.45 \leq A < 0.55$, (4) $0.55 \leq A < 0.65$. These windows approximately covered the amplitude ranges of the 30%, 40%, 50% and 60% subconductance levels. The 20% and 75% levels were excluded from this analysis because the corresponding peaks widely superimposed to the baseline and full open-state peaks. The values thus obtained were divided by the total number of observations, with the exclusion of those attributable to the baseline peak ($A < 0.25$) or peaks due to superimposed openings. Average values of these parameters, which provided an estimation of subconductance opening frequency, were plotted as a function of test potential (Fig. 5A). The plots revealed no major, regular dependence on membrane voltage of the frequency of subconductance occurrence for any of the levels considered. The frequencies measured for the different subconductance levels were also summed at each test potential, thus obtaining a global index of subconductance occurrence frequency. Also for this parameter no clear voltage dependence was observed (Fig. 5B).

Kinetic Properties of Subconductance Openings within Full-Size Bursts

To evaluate whether the kinetic behavior of intraburst subconductance openings was similar to or different from that of full-size openings, open and closed times were analyzed separately in both opening modes. We selected those subconductance openings in which the number of distinct dwellings in both the open and closed states was sufficiently high (>20 for each) to make a description of open- and closed-time distributions possible. This limited the analysis to a small number ($n = 6$) of intraburst subconductance openings. Open and closed times were concomitantly analyzed in the full-size burst openings during which the same subconductance openings occurred. This approach, which provided a comparison of dwell times between subconductance and full-size openings within individual bursts, was prompted by the observation that different bursts recorded at the same holding potential in a single patch can differ considerably in their kinetic behavior (Magistretti et al., 2003). In four of six cases, the open- and closed-time distribution of subconductance openings proved to be very similar to that of the corresponding full-size openings. Figure 6A illustrates one such case. Statistical analysis of mean open and closed times confirmed no significant differences between subconductance and full openings in these cases (Table 2, nos. 1–4). In two other subconductance openings, however, open- and/or closed-time distributions were clearly different from those of the corresponding full-size bursts. A representative example of this behavior is illustrated in Figure 6B, and statistical data are specified in Table 2 (nos. 5, 6). In the latter cases, open and closed times were also analyzed in other bursts recorded in the same patches at the same test potential in order to evaluate whether the kinetic pattern observed for subconductance openings was distinctive of conductance substates or also possibly shared by the full open state. An overall description of gating patterns was obtained by constructing scatter plots of theoretical mean open time

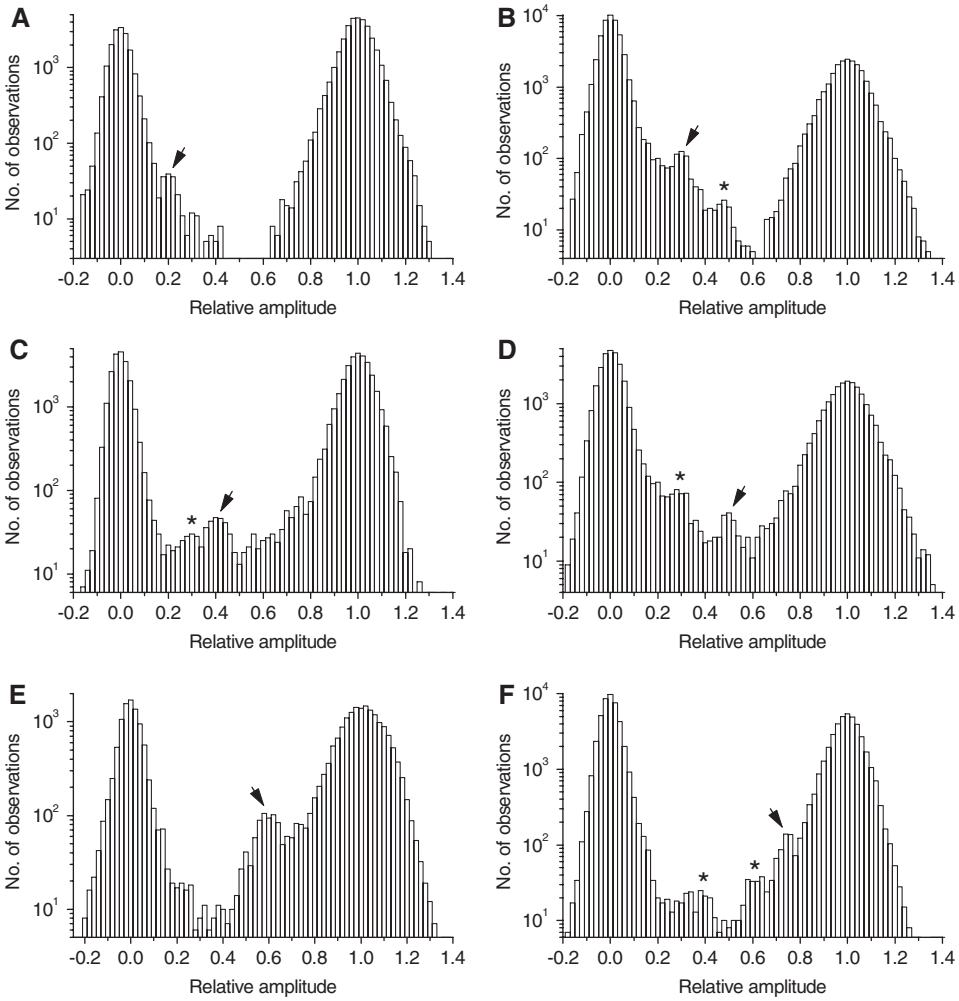

Fig. 4. Multiple subconductance peaks emerge in average amplitude histograms. The figure shows six current-amplitude histograms obtained from pooled data from different patches. The Patlak variance-mean analysis was employed to construct amplitude estimation histograms in individual patches at any given V_{test}. Then, current values of each histogram were normalized for the amplitude of the full-size channel opening, as derived by gaussian fitting of the corresponding peak. Normalized data from various patches were used to construct overall amplitude estimation histograms by summing the numbers of observations at each bin. Each overall histogram was obtained from those individual histograms that showed subconductance peaks at similar relative amplitude levels. The data used to construct the histograms were from eight different patches in *A* and *B*, six patches in *C*, five patches in *D*, four patches in *E* and 11 patches in *F*. *Arrows* point to peaks corresponding to various subconductance levels, with relative amplitudes of ~0.2 (*A*), ~0.3 (*B*), ~0.4 (*C*), ~0.5 (*D*), ~0.6 (*E*) and ~0.75 (*F*). *Arrows* point to the main subconductance peaks. Additional peaks, corresponding to the emergence of other subconductance levels, were also present sometimes and are indicated by *asterisks*. Note the logarithmic scale of the *y* axis.

($\bar{\tau}_o$) as a function of mean closed time ($\bar{\tau}_c$) (*see* Fig. 6C), in which each data point corresponded to a single full burst opening or intraburst subconductance opening. By adopting this approach, we found that in one case (Table 2, no. 5) the open-time distribution of the subconductance opening, although different from that of the full-size opening during which it occurred, was very similar to that observed in other full-size openings recorded in the same patch (*not shown*). However, in the other case (Table 2, no. 6), the kinetic pattern of intraburst subconductance openings appeared to be distinct from that observed in most full-size openings, as illustrated in Figure 6C. Note that in this instance no full size burst showed a similar, simultaneous occurrence of low mean closed time and high mean open time as the subconductance opening.

The above findings show that during an intraburst subconductance opening the kinetic behavior of the full-size burst opening can either be maintained or transiently replaced by a different one. They also suggest that, occasionally, channel substates can gate according to distinctive kinetic patterns that are not shared by full-size openings.

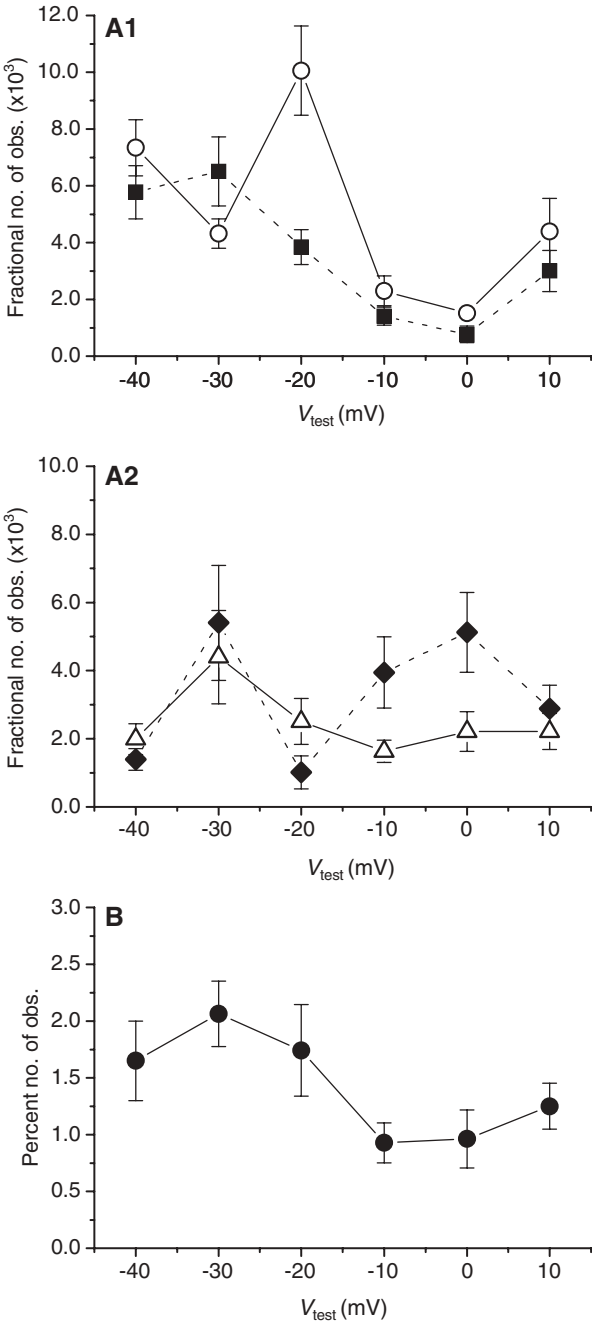

Fig. 5. Voltage dependence of channel probability to dwell in subconductance levels during burst openings. Amplitude estimation histograms, constructed according to the Patlak variance-mean analysis in individual patches at each V_{test}, were used to estimate the fraction of total open time spent by channels in each one of the identified subconductance levels. To obtain these estimations, numbers of observations in a defined relative-amplitude window were summed and divided by the total number of observations, with the exclusion of those attributable to the baseline peak (details are provided in Results). Data obtained at the same V_{test} were averaged among different patches. (*A*) The average fractional numbers of observations attributable to the 30% and 40% subconducance levels (*A1*, *open circles* and *filled squares*, respectively) and to the 50% and 60% subconducance levels (*A2*, *open triangles* and filled diamonds, respectively) are plotted as a function of V_{test}. (*B*) Plot of the average fractional numbers of observations attributable to all of the above subconductance levels as a function of V_{test}. In all plots, *n* was 7 at −40 m*V*, 16 at −30 m*V*, 13 at −20 m*V*, 9 at −10 m*V* and 0 m*V* and 7 at +10 m*V*.

Openings at Low Conductance Levels as Isolated Events

Examination of experimental tracings also revealed that openings characterized by lower amplitude than that of the full open state occasionally occurred separately from full-size burst openings (Fig. 7). These isolated low-conductance openings were then analyzed by following the two analytical approaches (methods 1 and 2) described above. Method 1 revealed that openings of similar amplitude relative to the full-size opening were often present at different test potentials in individual patches (Fig. 8A). Also in this case, therefore, the measurements of low-conductance opening amplitude, normalized to full-size opening amplitude, were pooled even if obtained at different test potentials. The histogram of relative amplitudes revealed six distinct peaks (Fig. 8B), corresponding to approximately 20%, 30%, 40%, 50%, 60% and 75% of the full-size opening amplitude. *I-V* plots were also constructed for each of the subconductance levels thus identified (Fig. 8C). Linear regressions to data points returned similar values of extrapolated reversal potential for all subconductance levels and the fully open state. Relative amplitudes of subconductance levels, measured using slope coefficients returned by linear regressions, were 0.202, 0.29, 0.385, 0.475, 0.59 and 0.77 (see Fig. 8C, legend). Again, these values compare favorably with the estimations obtained from the analysis of pooled relative-amplitude data.

Method 2 was applied after selecting tracing segments in which low-conductance openings appeared in isolation. Histograms of amplitude estimates were thus obtained, each one being constructed using data from openings recorded in a single patch at the same test potential (Fig. 9B, open columns). The histograms showed peaks corresponding to low-conductance levels that were fitted with gaussian functions. Histograms of amplitude estimates from full-size burst openings were also obtained separately with the same method and fitted with gaussian functions. The mean value (μ) returned by fitting a given low-conductance peak was always divided by the mean value of the corresponding full open state peak, to obtain a relative amplitude measurement. Data from several histograms were used to calculate average values for the relative amplitude of low-conductance openings, which are specified in Table 1. It can be seen that also this approach revealed relative amplitude levels

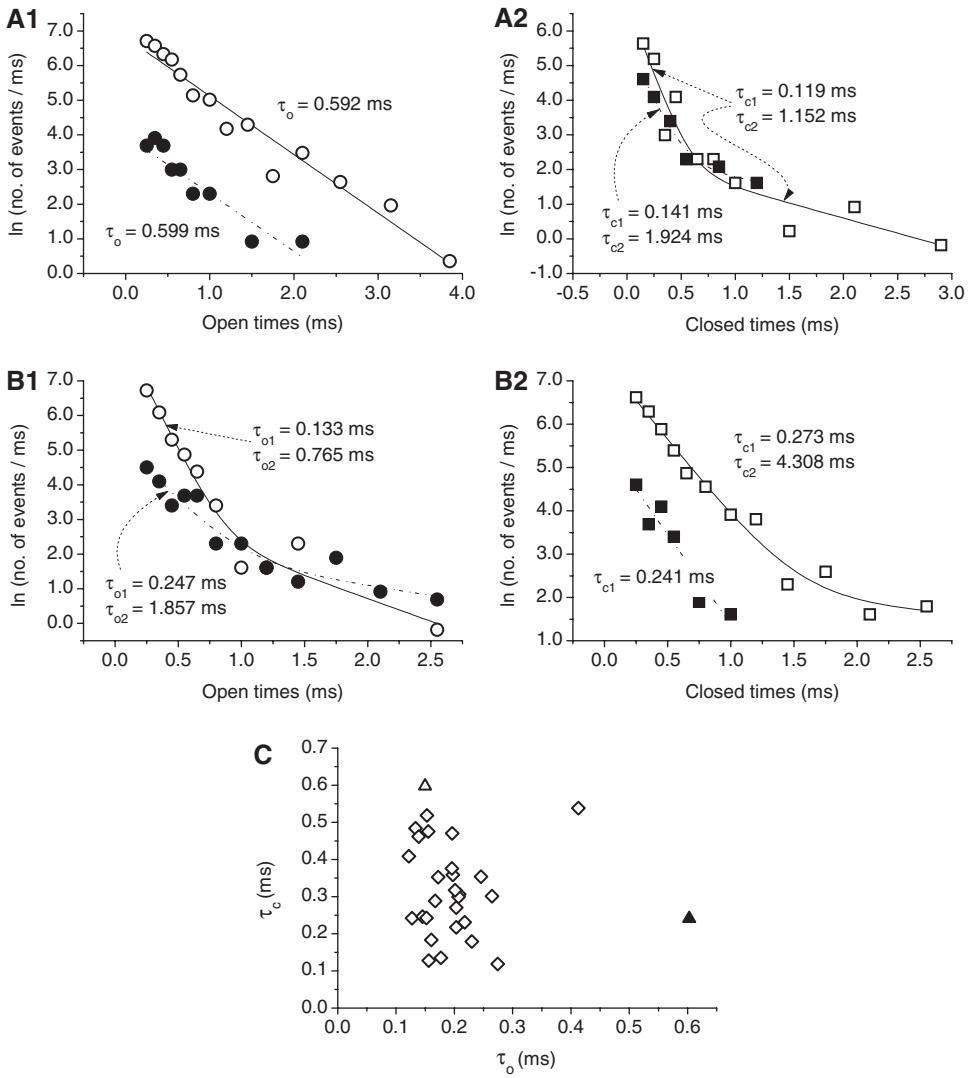

Fig. 6. Kinetic analysis of intraburst subconductance openings may reveal similarities or differences with respect to full-size burst openings. (*A*) Frequency-distribution diagrams of open times (*A1*) and closed times (*A2*) for an intraburst subconductance opening recorded at −40 m*V* (*filled symbols*) and the full-size burst opening during which the same subconductance opening occurred (*open symbols*). The subconductance opening here analyzed is the same as that shown in Figure 3*A1*, inset (patch A8618). (*B*) Frequency-distribution diagrams of open times (*B1*) and closed times (*B2*) for another intraburst subconductance opening recorded at −40 m*V* (*filled symbols*) and the full-size burst opening during which the same subconductance opening occurred (*open symbols*). The subconductance opening here analyzed is the same as that shown in Figure 1, no. 2 (patch B8708). The original dwell-time data were binned logarithmically as explained in Materials and Methods, and plots are shown here in a log-linear scale. The *x* value of each point is the logarithmic midpoint of the corresponding bin. Continuous lines are first- (*A1*, *B2*) or second- (*A2*, *B1*, *B2*) order exponential functions obtained by applying the fitting function of Eq. 2 (Materials and Methods). Time constant values returned by fittings are also specified. Note that the time constants describing open and closed times distributions are very similar for the subconductance opening and the corresponding full-size burst opening in *A* but clearly different in *B*. (*C*) Scatter plot of theoretical mean closed time ($\bar{\tau}_c$) as a function of theoretical mean open time ($\bar{\tau}_o$) for single bursts recorded at −40 m*V* in the same patch from which the data illustrated in *B* originated. $\bar{\tau}_o$ and $\bar{\tau}_c$ values were calculated according to Eq. 3 (Materials and Methods). Each *open symbol* corresponds to a single full-size burst opening. The *filled triangle* corresponds to the subconductance opening illustrated in *A* and the *open triangle*, to the full-size burst opening during which the same subconductance opening occurred.

very similar to those found for intraburst subconductance openings. Therefore, low-conductance openings were interpreted as isolated openings in a conductance substate of the same channels generating full-size burst openings.

Multiple Conductance Levels in Early, Transient Openings

Finally, the possible existence of multiple conductance levels was investigated in early, transient channel

Table 2. Open and closed times during intraburst subconductance openings: a comparison with full-size burst openings

Level	Patch	V_{test} (mV)	Substate relative amplitude	Open times (ms)		Closed times (ms)	
				Substate	Full-size burst	Substate	Full-size burst
1	A8618	−40	0.324	0.576 ± 0.105 (25)	0.576 ± 0.026 (483)	0.317 ± 0.062 (24)	0.315 ± 0.061 (63)
2	B9n01	−10	0.53	3.123 ± 0.389 (22)	3.934 ± 0.649 (41)	1.315 ± 0.452 (21)	1.3 ± 0.328 (40)
3	A9n09	0	0.613	1.455 ± 0.187 (55)	1.629 ± 0.137 (102)	0.15 ± 0.032 (22)	0.147 ± 0.025 (35)
4	B9n03	−30	0.316	1.755 ± 0.584 (22)	1.309 ± 0.087 (190)	0.26 ± 0.041 (21)	0.319 ± 0.035 (37)
5	B9n03	−30	0.336	1.643 ± 0.45 (21)	0.888 ± 0.129 (67)*	0.35 ± 0.043 (20)	0.541 ± 0.122 (23)
6	B8708	−40	0.289	0.515 ± 0.08 (47)	0.27 ± 0.015 (260)***	0.258 ± 0.031 (45)	0.383 ± 0.021 (342)*

The table shows average open and closed times for six different intraburst subconductance openings. For each subconductance opening, average open and closed times for the corresponding full-size burst opening during which it occurred are also specified for comparison. Values are mean ± SEM; numbers in parentheses are numbers of observations. Average open and closed times were calculated from raw dwell times. The statistical significance of differences between subconductance openings and full-size burst openings was evaluated by means of the two-tailed Student's t-test for unpaired data. $P <$ *0.05 and ***0.001. Note that subconductance openings 1 and 6 of this table are the same as illustrated in Figures 6A and 6B, respectively.

activity responsible for I_{NaT}. For this purpose, current recordings obtained by applying 50-ms step depolarizations at −30 to −10 mV were analyzed. In 11 patches, the recorded Na^+-channel activity was classified as of the purely "transient" type, as a consequence of the almost complete absence of "persistent" openings. In six of these patches, close inspection of experimental tracings revealed more than one conductance level. Exemplary tracings from the latter recordings are shown in Figure 10A. At least two conductance levels (horizontal dashed lines) could be observed. In some cases, smaller, additional conductance levels were also occasionally seen (Fig. 10A4, asterisk). Due to the short duration of early, transient openings, the variance-mean Patlak analysis, which requires opening events to be long enough relative to the sliding "window" of consecutive sample points on which calculations are made, could not be applied in this case. Therefore, simple current-amplitude histograms were constructed for the analysis of conductance levels of early, transient openings. Figure 10B1 shows one such histogram (data are from the experiment illustrated in Fig. 10A1). Besides a dominant current peak at −0.943 pA, an additional peak was revealed that appeared as a shoulder superimposed to the right part of the main peak (arrow). Figure 10B2 shows a global histogram constructed by pooling normalized data from the six above patches. The conductance peak could be properly fitted with a double gaussian function, with mean (μ) values of ∼1.02 and ∼1.35. Hence, at least two conductance levels were present among early, transient openings, the more represented of the two being in an approximate 0.75:1 amplitude ratio with the other.

Discussion

The data presented here show that voltage-gated Na^+ channels from native neurons can generate, during "persistent" activity, a multiplicity of subconductance levels in addition to a dominant, full-size opening level. These results add to the previous reports of multiple Na^+-channel substates in other cell preparations (Nagy, 1987; Patlak, 1988; Schreibmayer et al., 1989; Schreibmayer & Jeglitsch, 1992) insofar as they were obtained in pharmacologically untreated channels, in which the possible action of gating modifiers in inducing or altering substate openings is not a concern. We could document at least six distinct subconductance levels, with amplitudes ranging from ∼20% to ∼75% that of the fully open state. Moreover, since in amplitude estimation histograms the standard deviation of the peak corresponding to the fully open state was always considerably higher than that of the baseline peak, it cannot be excluded that additional subconductance levels of greater amplitude also exist, thus possibly superimposing to, and partially contaminating, the fully open state peak.

Another novel contribution of the present study is the fact that for the first time intraburst subconductance openings and isolated substate openings (i.e., those occurring separately from full-size burst openings) were analyzed independently and subsequently compared. Because in both cases very similar subconductance levels were revealed, the results of this approach strongly support the notion that the same population of channels can underlie both types of events. Persistent Na^+-channel openings of low conductance (about one-third that of full openings) occasionally occurring in inside-out patches from neocortical neurons had already been suggested to correspond to substate openings by Alzheimer, Schwindt & Crill (1993). Also, the low-conductance persistent openings reported in cerebellar Purkinje neurons as an elementary correlate of I_{NaP} (Sugimori, Kay & Llinás, 1994) can now be interpreted as likely reflecting substate openings.

The occurrence of intraburst subconductance openings was found to be largely independent of

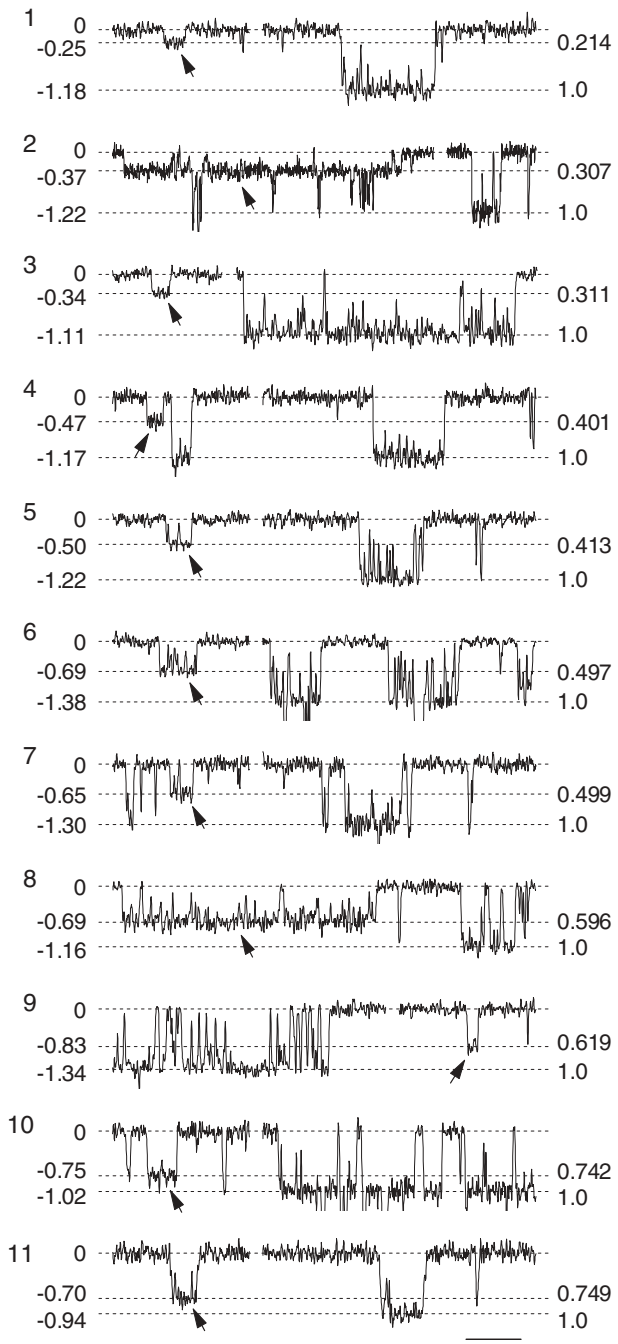

Fig. 7. Multiple low-conductance amplitude levels in isolated openings. The figure shows 11 representative examples of low-conductance openings (*arrows*) occurring separately from full-size burst openings. For each low-conductance opening, a representative full-size opening recorded in the same patch is also shown for comparison. Recordings were made in 10 different patches at various V_{test}s (−40 to −20 mV). The numbers to the left of each tracing are absolute current levels (pA). The numbers to the right of each tracing represent relative amplitude values (with the amplitude of full-size openings made equal to 1.0). *x*-axis calibration bar = 20 ms for all tracings except 2 (40 ms).

membrane potential in the −40 to +10 mV window. Similarly, the frequency and mean duration of full-size "persistent" burst openings was reported to be largely voltage-independent (Magistretti & Alonso, 2002), whereas the bulk of I_{NaP} voltage dependence was found to be underlain by that of intraburst mean open and closed times (Magistretti & Alonso, 2002). Moreover, we found that the whole percent contribution of subconductance openings to the total channel open time never exceeded 2% (*see* Fig. 5B). Therefore, the probability of subconductance opening occurrence during "persistent" activity is unlikely to give a significant contribution to the voltage dependence of I_{NaP}.

Our analysis of channel kinetic behavior during subconductance openings also revealed some unexpected complexity. Although in most cases the kinetic pattern of open and closed times of an intraburst subconductance opening largely reproduced that of the full burst opening during which it occurred, in some other cases it appeared clearly different. Therefore, a subconductance opening that interrupts a full-size opening does not necessarily correspond to the perpetuation of a single gating event at a lower conductance level but can sometimes represent a shift to an entirely different gating modality. Moreover, we also found that, occasionally, subconductance openings may gate according to kinetic patterns that are not shared by full-size burst openings recorded in the same conditions. The existence of multiple gating modalities, in terms of kinetic behavior, in voltage-gated Na^+ channels has already been reported in neuronal and nonneuronal cells (Patlak & Ortiz, 1989; Magistretti et al., 2003). The present results suggest that some of these multiple gating modes may be preferentially associated with subconductance openings.

Finally, we found that at least two distinct conductance levels, and probably more, can be detected in the early, fast-inactivating Na^+-channel activity responsible for the transient Na^+-current component (I_{NaT}). The two main conductance levels were in an approximate 0.75:1 amplitude ratio, and the lower-amplitude one was the more frequently observed. Two distinct conductance levels in a very similar amplitude ratio were also described by Nagy, Kiss & Hof (1983) for fast-inactivating Na^+ channels of neuroblastoma cells. The lower conductance level, which we found to predominate among early openings, could correspond to the 75% conductance levels observed in "persistent" burst openings. Thus, a single subconductance level could be differently represented during distinct Na^+-channel gating modalities ("transient" *vs.* "persistent"). These findings may be interesting in light of the fact that a lower conductance for "transient" than for "persistent" Na^+-channel openings (∼15 *vs.* ∼20 pS, respectively) has been observed in entorhinal cortex neurons (Magistretti et al., 1999a, 1999b) but not in neocortical neurons (Alzheimer et al., 1993). A higher probability of channel gating in the 75% conductance level during early openings than during later open-

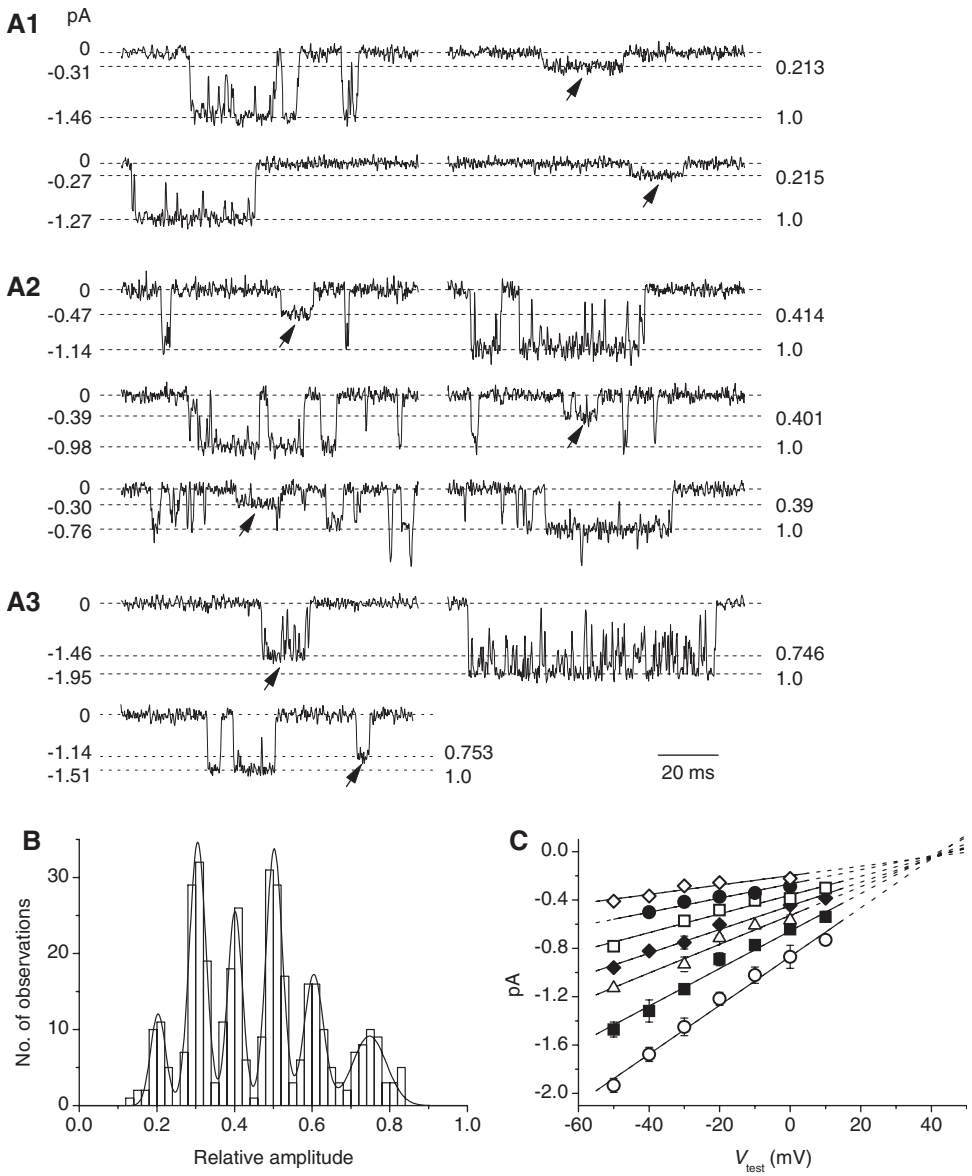

Fig. 8. Identification of multiple, discrete conductance levels among isolated low-conductance openings. (*A*) Examples of visually identified isolated low-conductance openings (*arrows*) recorded at various V_{test}s in three different patches (B9n08 in *A1*, A9n05 in *A2*, B8616 in *A3*). V_{test}s were −30 m*V* in *A1* (*top*) and −20 m*V* in *A1* (*bottom*); −20 m*V* in *A2* (*top*), −10 m*V* in *A2* (*middle*) and 0 m*V* in *A2* (*bottom*); −50 m*V* in *A3* (*top*) and −30 m*V* in *A3* (*bottom*). The numbers to the left of each tracing are absolute current levels (pA). The numbers to the right of each tracing represent relative amplitude values (with the amplitude of full-size openings made equal to 1.0). Note that low-conductance openings of similar amplitudes relative to full-size openings were observed in a single patch regardless by the different V_{test}s. (*B*) Frequency-distribution diagram of relative amplitudes of visually identified low-conductance openings. Amplitude values are expressed as normalized to those of full-size openings. The data were obtained from 23 different patches, and measurements made at different V_{test}s were pooled. The histogram was best fit with the sum of five gaussian functions (see Eq. 1). Mean (μ) values returned by fitting were 0.305, 0.401, 0.502, 0.604 and 0.748. (*C*) Average *I-V* plots of subconductance levels and the fully open state. Subconductance openings that fell within one of the peaks of the histogram in *B* (specifically, with an amplitude comprised within the interval μ ± 0.05) were selected, average values were obtained in each patch, then averaged among patches and plotted as a function of V_{test}. Each point is the average of measures made in two to nine patches, error bars are standard deviation (SD; where the error bar is not visible, SD is smaller than the size of the symbol). Slope conductance and extrapolated reversal-potential values were obtained by linear regression of data points (*straight lines*) and were 20.2 pS and +43.0 m*V*, respectively, for the fully-open state (*open circles*), 15.5 pS and +42.3 m*V* (*filled squares*), 11.9 pS and +44.4 m*V* (open triangles), 9.8 pS and +45.9 m*V* (*filled diamonds*), 7.8 pS and +38.5 m*V* (*open squares*), 5.9 pS and +45.7 m*V* (*filled circles*) and 4.1 pS and +47.7 m*V* (*open diamonds*).

ings, also observed in neuroblastoma cells (Nagy et al., 1983), could justify the lower conductance reported for transient Na^+-channel openings (Magistretti et al., 1999a, 1999b). Differences in channel probability of gating in the 75% conductance level during early, transient activity could also explain the

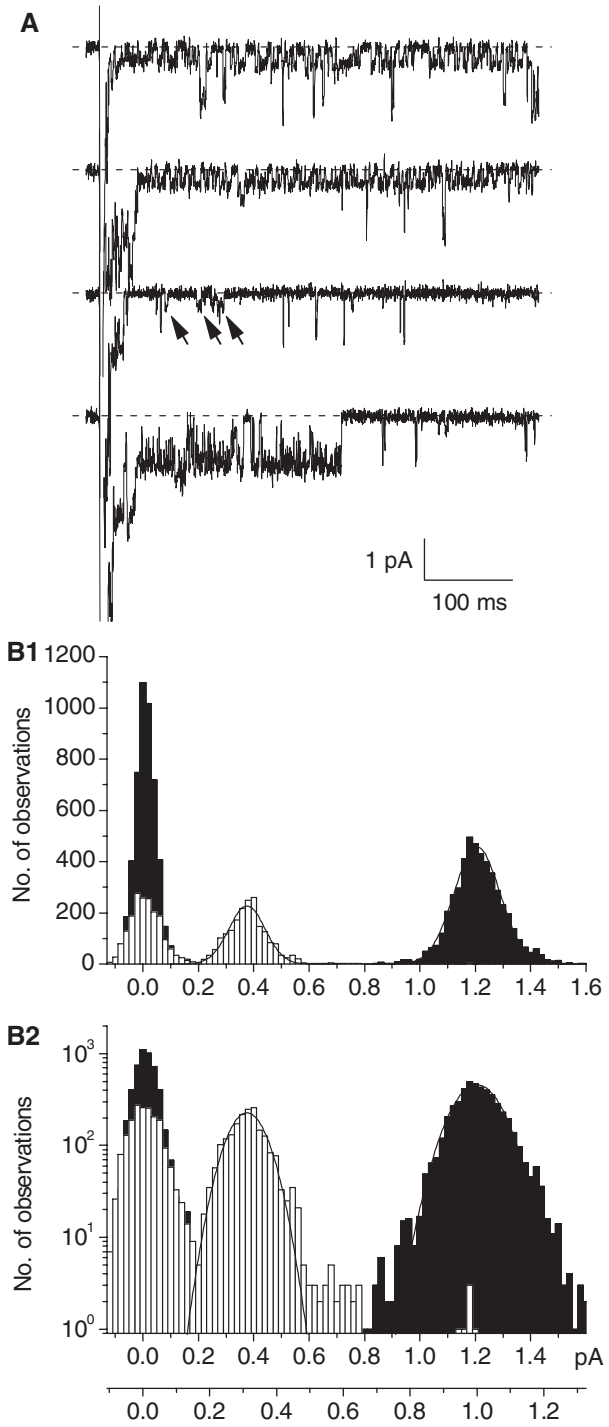

Fig. 9. Application of automated variance-mean analysis to low-conductance openings occurring independently of full-size burst openings. (*A*) Exemplary current sweeps recorded at $V_{test} = -20$ m*V* in a representative patch (D9n09). Prolonged (first and second tracings) and short (third tracing, *arrows*) low-conductance openings were occasionally observed in addition to full-size burst openings (fourth tracing). (*B*) Histograms of amplitude estimates obtained by applying the Patlak variance-mean analysis to the experiment illustrated in *A*. *Open bars* are data from low-conductance openings, *filled bars* are data from full-size burst openings recorded in the same patch. In *B1* and *B2*, numbers of observations are given in linear scale and logarithmic scale, respectively. Smooth lines are gaussian fittings of the low-conductance and full-opening peaks. Fitting parameters are $A_1 = 37.02$, $\mu_1 = 0.376$ pA, $\sigma_1 = 0.065$ pA; $A_2 = 95.18$, $\mu_2 = 1.206$ pA, $\sigma_2 = 0.083$ pA. In the lower *x* axis in *B2* current values have been normalized to the mean amplitude of full-size openings.

discrepant results from different neuronal populations.

In conclusion, the results illustrated here show that pharmacologically untreated Na^+ channels from native neurons can generate a variety of conductance substates and suggest that substate openings may influence differently the multiple gating modes displayed by these channels.

This study was partly supported by a grant (PRIN 2005, 2005059453_003) from the Italian Ministry of Education, University and Research to J. M.

References

Alzheimer, C., Schwindt, P.C., Crill, W.E. 1993. Modal gating of Na^+ channels as a mechanism of persistent Na^+ current in pyramidal neurons from rat and cat sensorimotor cortex. *J. Neurosci.* **13:**660–673

Blatz, A.L., Magleby, K.L. 1986. Quantitative description of three modes of activity of fast chloride channels from rat skeletal muscle. *J. Physiol.* **378:**141–174

Chinn, K., Narahashi, T. 1986. Stabilization of sodium channel states by deltamethrin in mouse neuroblastoma cells. *J. Physiol.* **380:**191–207

Colquhoun, D., Sigworth, F.J. 1995. Fitting and statistical analysis of single channel records. *In:* Sakmann, B., Neher, E., (eds) Single Channel Recording. pp 483–587, Plenum Press, New York

Fox, J.A. 1987. Ion channel subconductance states. . *J. Membr. Biol.* **97:**1–8

Green, W.N., Weiss, L.B., Andersen, O.S. 1987. Batrachotoxin-modified sodium channels in planar lipid bilayers. Ion permeation and block. *J. Gen. Physiol.* **89:**841–872

Magistretti, J., Alonso, A. 2002. Fine gating properties of channels responsible for persistent sodium current generation in entorhinal cortex neurons. *J. Gen. Physiol.* **120:**855–873

Magistretti, J., de Curtis, M. 1998. Low-voltage activated T-type calcium currents are differently expressed in superficial and deep layers of guinea pig piriform cortex. *J. Neurophysiol.* **79:**808–816

Magistretti, J., Ragsdale, D.S., Alonso, A. 1999a. High conductance sustained single channel activity responsible for the low threshold persistent Na^+ current in entorhinal cortex neurons. *J. Neurosci.* **19:**7334–7341

Magistretti, J., Ragsdale, D.S., Alonso, A. 1999b. Direct demonstration of persistent Na^+ channel activity in dendritic processes of mammalian cortical neurones. *J. Physiol.* **521:**629–636

Magistretti, J., Ragsdale, D.S., Alonso, A. 2003. Kinetic diversity of single-channel burst openings underlying persistent Na^+ current in entorhinal cortex neurons. *Biophys. J.* **85:**3019–3034

McManus, O.B., Blatz, A.L., Magleby, K.L. 1987. Sampling, log binning, fitting, and plotting durations of open and shut intervals from single channels and the effects of noise. *Pfluegers Arch.* **410:**530–553

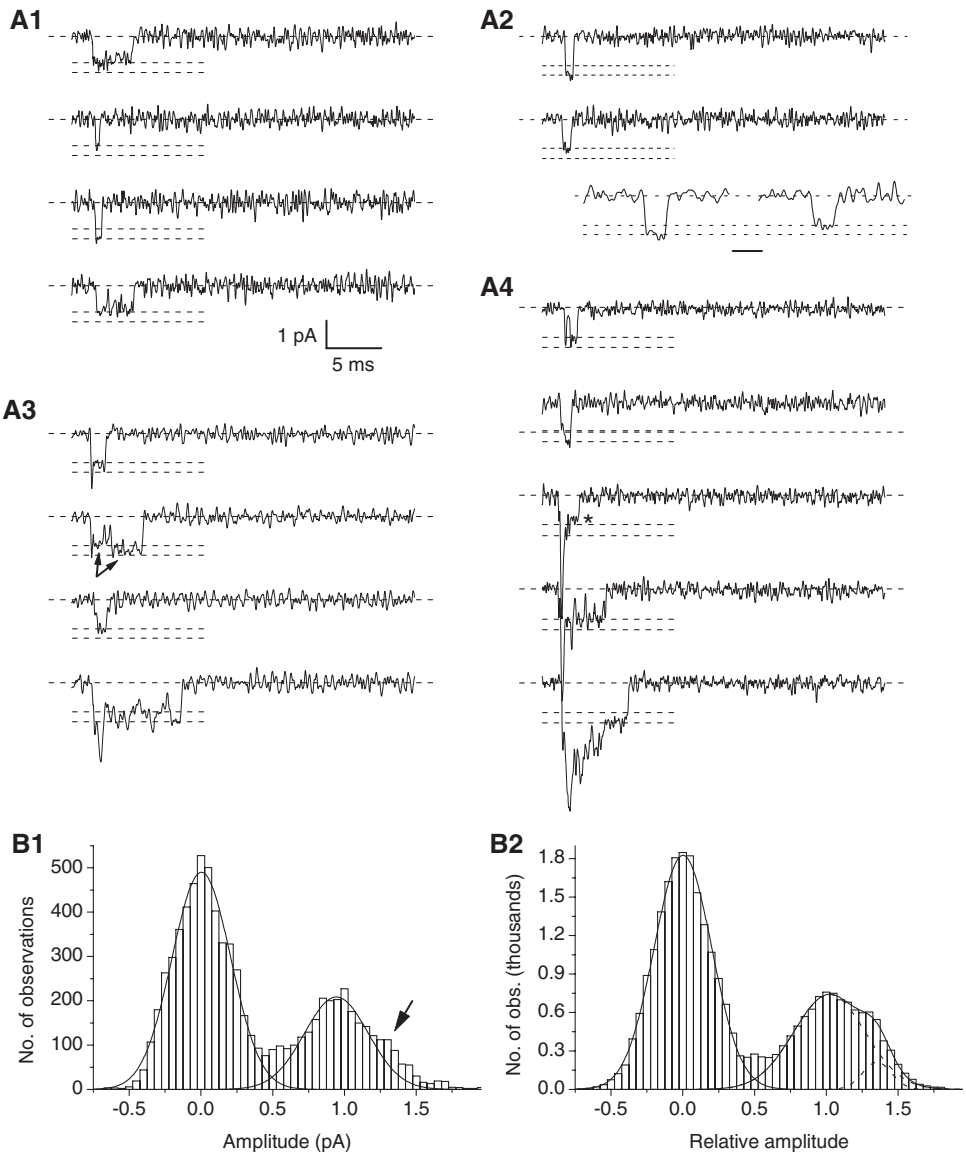

Fig. 10. Two conductance levels in early, transient openings. (*A*) Exemplary single-channel current tracings recorded in response to 50-ms depolarizing pulses in four different patches (A8714 in *A1*, B8717 in *A2*, C8710 in *A3*, D8710 in *A4*). V_{test} was −30 m*V* in all cases. The *horizontal dashed lines* mark the two main amplitude levels observed in each recording. In the lower part of *A2*, two representative openings have been placed side by side and are shown in an expanded time scale (calibration bar = 1 ms) to highlight the difference in amplitude. The double arrow in A3 points to a shift from the low to the high amplitude level within a single opening. (*B*) Current-amplitude histograms for the data exemplified in *A*. *B1* is the histogram obtained from a single representative experiment (patch A8714). *Smooth lines* are gaussian fittings of the baseline peak and the main conductance peak. Fitting parameters for the main conductance peak are $A = 116.44$, $\mu = 0.943$ pA, $\sigma = 0.228$ pA (fitting was limited to the 0.70–1.15 pA amplitude window). Note that an additional peak was revealed as a shoulder superimposing to the right part of the main conductance peak (*arrow*). *B2* is the global histogram obtained by pooling data from six different patches, after normalizing current values of each recording for the amplitude of the corresponding main conductance peak. The baseline peak and the conductance peak were separately fitted with a single and a double gaussian function, respectively (*smooth, continuous lines*). Fitting parameters for the conductance peak are $A_1 = 461.26$, $\mu_1 = 1.022$, $\sigma_1 = 0.249$; $A_2 = 53.4$, $\mu_2 = 1.354$, $\sigma_2 = 0.101$ (the two components of the double gaussian function are also shown separately as *dashed lines*).

Meves, H., Nagy, K. 1987. Multiple conductance states of the sodium channel and of other ion channels. *Biochim. Biophys. Acta* **988:**99–105

Nagy, K. 1987. Subconductance states of single sodium channels modified by chloramine-T and sea anemone toxin in neuroblastoma cells. *Eur. Biophys. J* **15:**129–132

Nagy, K., Kiss, T., Hof, D. 1983. Single Na channels in mouse neuroblastoma cell membrane. Indications for two open states. *Pfluegers Arch.* **399:**302–308

Naranjo, D., Latorre, R. 1993. Ion conduction in substates of the batrachotoxin-modified Na^+ channel from toad skeletal muscle. *Biophys. J.* **64:**1038–1050

Nilius, B., Vereecke, J., Carmeliet, E. 1989. Subconductance states in cardiac sodium channels. *Biomed. Biochim. Acta.* **48:**S354–S357

Patlak, J.B. 1988. Sodium channel subconductance levels measured with a new variance-mean analysis. *J. Gen. Physiol.* **92:**413–430

Patlak, J.B., Ortiz, M. 1989. Kinetic diversity of Na+ channel bursts in frog skeletal muscle. *J. Gen. Physiol.* **94:**279–301

Ravindran, A., Schild, L., Moczydlowski, E. 1991. Divalent cation selectivity for external block of voltage-dependent Na^+ channels prolonged by batrachotoxin. Zn^{2+} induces discrete substates in cardiac Na^+ channels. *J. Gen. Physiol.* **97:**89–115

Schild, L., Ravindran, A., Moczydlowski, E. 1991. Zn^{2+}-induced subconductance events in cardiac Na^+ channels prolonged by batrachotoxin. Current-voltage behavior and single-channel kinetics. *J. Gen. Physiol.* **97:**117–142

Schreibmayer, W., Jeglitsch, G. 1992. The sodium channel activator brevetoxin−3 uncovers a multiplicity of different open states of the cardiac sodium channel. *Biochim. Biophys. Acta.* **1104:**233–242

Schreibmayer, W., Tritthart, H.A., Schindler, H. 1989. The cardiac sodium channel shows a regular substate pattern indicating synchronized activity of several ion pathways instead of one. *Biochim. Biophys. Acta.* **986:**172–186

Sigel, E. 1987. Effects of veratridine on single neuronal sodium channels expressed in Xenopus oocytes. *Pfluegers Arch.* **410:**112–120

Sigworth, F.J., Sine, S.M. 1987. Data transformations for improved display and fitting of single-channel dwell time histograms. *Biophys. J.* **52:**1047–1054

Sugimori, M., Kay, A.R., Llinás, R. 1994. The persistent Na^+ channel in cerebellar Purkinje cells has a single channel conductance distinct from the inactivating current. *Soc. Neurosci. Abstr.* **20:**63